Oxygen Atom Transfer in Models for Molybdenum Enzymes: Isolation and Structural, Spectroscopic, and Computational Studies of Intermediates in Oxygen Atom Transfer from Molybdenum(VI) to Phosphorus(III)

Andrew J. Millar,[a] Christian J. Doonan,[a] Paul D. Smith,[a] Victor N. Nemykin,[b] Partha Basu,*[b] and Charles G. Young*[a]

Abstract: Intermediates in the oxygen atom transfer from Mo^{VI} to P^{III}, [$Tp^{iPr}MoOX(OPR_3)$] (Tp^{iPr} = hydrotris(3-isopropylpyrazol-1-yl)borate; X = Cl^-, phenolates, thiolates), have been isolated from the reactions of [$Tp^{iPr}MoO_2X$] with phosphines (PEt_3, $PMePh_2$, PPh_3). The green, diamagnetic oxomolybdenum(IV) complexes possess local C_1 symmetry (by NMR spectroscopy) and exhibit IR bands assigned to ν(Mo=O) (approximately 950 cm^{-1}) and ν(P=O) (1140–1083 cm^{-1}) vibrations. The X-ray crystal structures of [$Tp^{iPr}MoOX(OPEt_3)$] (X = OC_6H_4-2-*s*Bu, S*n*Bu), [$Tp^{iPr}MoO(OPh)(OPMePh_2)$], and [$Tp^{iPr}MoOCl(OPPh_3)$] have been determined. The monomeric complexes exhibit distorted octahedral geometries, with coordination spheres composed of tridentate *fac*-Tp^{iPr} and mutually *cis* monodentate terminal oxo, phosphoryl (phosphine oxide), and monoanionic X ligands. The electronic structures and stabilities of the complexes have been probed by computational methods, with the three-dimensional energy surfaces confirming the existence of a low-energy steric pocket that restricts the conformational freedom of the phosphoryl ligand and inhibits complete oxygen atom transfer. The reactivity of the complexes is also briefly described.

Keywords: bioinorganic chemistry · electronic structure · molybdenum · oxygen atom transfer · phosphoryl ligands

Introduction

Molybdenum enzymes are widely distributed in nature, are essential in key metabolic processes, and are active agents in the global biogeochemical cycles of elements such as carbon, nitrogen, and sulfur.[1] The pterin-containing enzymes feature mononuclear oxomolybdenum active states and generally catalyze *net* oxygen atom transfer (OAT) reactions. Net OAT is also a defining reaction in synthetic oxomolybdenum chemistry.[2–6]

The mechanisms of enzymes from the sulfite oxidase and dimethyl sulfoxide (DMSO) reductase families are thought to involve *direct* OAT between the substrate and the Mo center.[1] Evidence for this has been garnered through (inter alia) protein structural,[7] spectroscopic,[8] kinetics,[9,10] and theoretical[11] studies. Sulfite oxidases and assimilatory nitrate reductases effect substrate transformations through interconversion of $Mo^{VI}O[O]$ ([O] = active oxygen) and $Mo^{IV}O$ centers, while members of the DMSO reductase family exploit $Mo^{VI}[O]$ and Mo^{IV} centers in their catalytic cycles. An intermediate in the oxidation of dimethylsulfide (DMS) by *Rhodobacter capsulatus* DMSO reductase has been isolated and structurally characterized by McAlpine et al.[7c]

Model systems containing dithiolene, trispyrazolylborate, and NS-/NO-donor coligands emulate enzymatic OAT reactions, with the stoichiometric or catalytic oxidation of tertiary phosphines being an archetypal OAT reaction.[2–6] Reactions of this type are generally second order, with rate constants in the range 2×10^{-6}–22 $M^{-1}s^{-1}$, depending on the

[a] Dr. A. J. Millar, Dr. C. J. Doonan, Dr. P. D. Smith, Prof. C. G. Young
School of Chemistry
University of Melbourne, Victoria, 3010 (Australia)
Fax: (+61) 3-9347-5180
E-mail: cgyoung@unimelb.edu.au

[b] Dr. V. N. Nemykin, Prof. P. Basu
Department of Chemistry and Biochemistry
Duquesne University, Pittsburgh, PA 15282 (USA)
Fax: (+1) 412-396-5683
E-mail: basu@duq.edu

Supporting information for this article (full listings of analytical and spectroscopic data for all compounds reported, three-dimensional energy surfaces and energy surface contour maps) is available on the WWW under http://www.chemeurj.org/ or from the author.

 DOI: 10.1002/chem.200401101

nature of the coligands.[4] Kinetics data are consistent with associative reaction mechanisms initiated by nucleophilic attack of the phosphine lone pair on a π* Mo=O orbital producing a phosphine oxide intermediate that rapidly transforms into product. Oxidation of the Mo^{IV} by-product by, for example, DMSO, permits the development of catalytic systems based on direct, bidirectional OAT.[2–6] The demonstration by Schultz et al. that *Rhodobacter sphaeroides* DMSO reductase catalyzes OAT from DMSO to a water-soluble phosphine underscores the potential for model studies to inform about enzyme structure and reactivity.[10] However, apart from results from our laboratories,[12–14] there have been no reports of the interception or isolation of intermediates in Mo-mediated OAT reactions, including those of enzyme models.

The reactions of [Tp*MoO_2X] (Tp* = hydrotris(3,5-dimethylpyrazol-1-yl)borate; X = monoanion, especially SPh^-) with PPh_3 yield $OPPh_3$ and oxomolybdenum(IV) complexes by direct OAT.[15] These complexes are components of a broad-based model for the combined (catalytic) OAT and coupled electron–proton transfer (CEPT) reactions envisaged for enzymes.[16] Phosphine oxidation in this system has been probed by a number of computational studies.[17] In the first step of the reaction between *sterically unencumbered* [$MoO_2(SH)_2(NH_3)_2$] and PMe_3, nucleophilic attack of PMe_3 on a π* Mo=O orbital perpendicular to the MoO_2 unit and at an Mo–O···P angle of approximately 130° takes place. This results in a transition state with a weakened Mo–O bond (1.83 Å), an O–P interaction (2.43 Å), and an O=Mo-O-P torsion angle of 89.7°; the remaining Mo=O bond becomes stronger, consistent with a "spectator oxo" function.[18] The $OPMe_3$ ligand then rotates about the Mo–O bond, thereby breaking the Mo–O π interaction to generate an intermediate with Mo=O, Mo–O, and O–P distances of 1.67, 2.18, and 1.53 Å, respectively, and an O=Mo–O–P torsion angle of 0.5°. The intermediate is 288 kJ mol^{-1} lower in energy than the reactants. At this stage, displacement of $OPMe_3$ by water is predicted to take place by an *associative* mechanism, the loss of $OPMe_3$ being assisted by the absence of π interactions in the intermediate. Our isolation of oxo(phosphoryl) OAT intermediates[12,13] confirms their existence and provides a unique opportunity to experimentally evaluate the factors influencing their stability and reactivity.

Here, we report the isolation and characterization of the oxo(phosphoryl)molybdenum(IV) complexes, [$Tp^{iPr}MoOX(OPR_3)$] (Tp^{iPr} = hydrotris(3-isopropylpyrazol-1-yl)borate), generated by treating *cis*-dioxomolybdenum(VI) complexes with tertiary phosphines. Since complete OAT to phosphine is arrested in these Mo^{IV}–O=P^V complexes, they represent important intermediates along the reaction coordinate for OAT from Mo^{VI} to P^{III}. The structural, spectroscopic, and theoretical interrogation of intermediates of this type is essential for a complete understanding of Mo-mediated OAT reactions. Chemical, structural, and theoretical studies of the complexes are consistent with the stabilization of the complexes through stereoelectronic influences. Complexes **1**–**13** are described herein; preliminary results relating to complex **2** have appeared in a communication.[12] Complexes **2**, **6**, **7**, **9**, and **12** have been structurally characterized. Complex **13** is a computational model.

[$Tp^{iPr}MoOCl(OPEt_3)$] **1**

[$Tp^{iPr}MoO(OPh)(OPEt_3)$] **2**[12]

[$Tp^{iPr}MoO(OC_6H_4$-3-Me$)(OPEt_3)$] **3**

[$Tp^{iPr}MoO(OC_6H_4$-3-*t*Bu$)(OPEt_3)$] **4**

[$Tp^{iPr}MoO(OC_6H_3$-3,5-*t*$Bu_2)(OPEt_3)$] **5**

[$Tp^{iPr}MoO(OC_6H_4$-2-*s*Bu$)(OPEt_3)$] **6**

[$Tp^{iPr}MoO(S$*n*Bu$)(OPEt_3)$] **7**

[$Tp^{iPr}MoO(S$*s*Bu$)(OPEt_3)$] **8**

[$Tp^{iPr}MoO(OPh)(OPMePh_2)$] **9**

[$Tp^{iPr}MoO(OC_6H_4$-3-Me$)(OPMePh_2)$] **10**

[$Tp^{iPr}MoO(OC_6H_4$-4-Br$)(OP$*n*$Bu_3)$] **11**

[$Tp^{iPr}MoOCl(OPPh_3)$] **12**

[$Tp^{iPr}MoO(OPh)(OPPh_3)$] **13**

Results and Discussion

Syntheses: The reactions of [$Tp^{iPr}MoO_2X$] complexes with 1.5 equivalents of tertiary phosphines in noncoordinating solvents such as benzene or toluene resulted in incomplete OAT and the generation of oxo(phosphoryl)molybdenum(IV) species according to Equation (1). When the reactions were performed in coordinating solvents (solv) such as acetonitrile or *N*,*N*-dimethylformamide (DMF), complete OAT occurred and the equilibrium in Equation (2) was established. (In related work, we have demonstrated that these phosphine oxide displacement reactions from **2** and **9** proceed by a dissociative interchange mechanism.[19]) Reaction times varied from minutes for the thiolate derivatives to approximately 12–24 h for the phenolate derivatives. Isolation of the complexes was achieved by solvent removal, dissolution of the green (NCMe) or brown (benzene, toluene) residues in dry hexane, and cooling to induce crystallization. The position of the equilibrium in Equation (2) is solvent, concentration, and coligand dependent; only phosphoryl complexes were isolated by using the specified workup of the phenolate derivatives. However, their dissolution in acetonitrile led to in situ formation of [$Tp^{iPr}MoO(OAr)(NCMe)$] and free OPR_3, as evidenced by ^{1}H NMR spectroscopy (Ar = aryl). Slight modification of the workup allowed the isolation of either [$Tp^{iPr}MoOX(OPR_3)$] or [$Tp^{iPr}MoOX(solv)$] when X

was a thiolate; conversion of the latter to the former upon addition of OPR_3 and suitable work up facilitated the preparation of isotopically labeled complexes such as [Tp$^{i\mathrm{Pr}}$MoO(S*n*Bu)(^{18}OPEt$_3$)].

$$[Tp^{i\mathrm{Pr}}MoO_2X]+PR_3 \rightarrow [Tp^{i\mathrm{Pr}}MoO(OPR_3)X] \quad (1)$$

$$[Tp^{i\mathrm{Pr}}MoO(OPR_3)X]+solv \rightleftharpoons [Tp^{i\mathrm{Pr}}MoOX(solv)]+OPR_3 \quad (2)$$

The disparate outcomes of the reactions of [Tp$^{i\mathrm{Pr}}$MoO$_2$Cl] with P$^{\mathrm{III}}$ compounds underscore the versatility of this system. Thus, the reaction of [Tp$^{i\mathrm{Pr}}$MoO$_2$Cl] with phosphines or P(O*i*Pr)$_3$ in NCMe yields light green-blue colored [Tp$^{i\mathrm{Pr}}$MoOCl(NCMe)], while the reaction of [Tp$^{i\mathrm{Pr}}$MoO$_2$Cl] with phosphines in benzene affords the phosphoryl complexes **1** and **12**. However, the reaction of [Tp$^{i\mathrm{Pr}}$MoO$_2$Cl] with P(O*i*Pr)$_3$ in toluene leads to the formation of the unusual dinuclear species [(Tp$^{i\mathrm{Pr}}$MoOCl)(μ-O){Tp$^{i\mathrm{Pr}}$-MoO(OH)}].[20] Synthetic observations are consistent with the following qualitative ligand affinities: for the phenolate systems, $OPR_3 > MeCN \gg Tp^{i\mathrm{Pr}}MoO_2$ (comproportionation); for the thiolate systems, $MeCN, DMF \approx OPR_3 \gg Tp^{i\mathrm{Pr}}MoO_2$; when X = Cl, $MeCN > OPR_3 \gg Tp^{i\mathrm{Pr}}MoO_2$. (Note: mixtures of [Tp$^{i\mathrm{Pr}}$MoOX(OPEt$_3$)] and [Tp$^{i\mathrm{Pr}}MoO_2$X] (1:1) are stable with respect to comproportionation.) The reactions are quite general and a variety of other derivatives have been synthesized.[21,22]

The isolation of phosphoryl complexes of Tp$^{i\mathrm{Pr}}$ contrasts with the complete OAT generally observed between [Tp*MoO$_2$X] and tertiary phosphines. In reactions involving PEt$_3$, PPh$_3$, and P*n*Bu$_3$, dissociation of OPR_3 leads to the formation of solvent-bound or chelated oxomolybdenum(IV) complexes; subsequent solvent or comproportionation reactions can lead to mononuclear or dinuclear oxomolybdenum(V) complexes.[15,20] Interestingly, one Tp* complex, namely, [Tp*MoOCl(OPMe$_3$)], has now been isolated.[13] The enhanced stability of Tp$^{i\mathrm{Pr}}$ complexes over most Tp* analogues appears to be stereoelectronic in origin (see below).

The green- (OPEt$_3$ and OP*n*Bu$_3$) or gold-colored (OPMePh$_2$) phosphoryl complexes were moderately air-stable as solids but were stored under an inert atmosphere. However, they were extremely air-sensitive in solution and unstable in chlorinated solvents (see below). The complexes were soluble and stable in dried, deoxygenated toluene and benzene, but dissolution in coordinating solvents generated [Tp$^{i\mathrm{Pr}}$MoOX(solv)] species. They reacted with oxygen atom donors such as pyridine *N*-oxide, cyclohexene oxide, and DMSO to form the corresponding *cis*-dioxo complexes [Tp$^{i\mathrm{Pr}}$MoO$_2$X]. By analogy, reactions with propylene sulfide yielded red [Tp$^{i\mathrm{Pr}}$MoOSX], isolated either as monomeric or dimeric species.[21,23] Chlorinated solvents induced decomposition with the formation of the paramagnetic, EPR-active complexes [Tp$^{i\mathrm{Pr}}$MoOClX]; purple-brown [Tp$^{i\mathrm{Pr}}$MoOCl(OC$_6$H$_3$-3,5-*t*Bu$_2$)] was isolated and identified by IR (ν(Mo=O) = 966 cm^{-1}, ν(BH) = 2494 cm^{-1}) and EPR (g_{iso} = 1.948, $A_{Mo} = 47.11 \times 10^{-4}$ cm^{-1}) spectroscopy. The phenolate complexes were rapidly chlorinated (within minutes), whereas the thiolate complexes reacted slowly. Indeed, autoxidation of the thiolates was competitive with chlorination under aerobic conditions. Previous studies found that electrochemically produced oxomolybdenum(IV) thiolate complexes were more stable than their olate counterparts; this observation was ascribed to the greater stabilization of the soft Mo$^{\mathrm{IV}}$ center by thiolate donors.[24]

We were unable to obtain any evidence for the reversibility of Equation (1). Thus, mixtures of [Tp$^{i\mathrm{Pr}}$MoOCl(OPPh$_3$)] and [D$_{15}$]PPh$_3$ in [D$_6$]benzene monitored by ^{31}P NMR spectroscopy showed no growth of resonances attributable to PPh$_3$ or [D$_{15}$]OPPh$_3$. Only slow dissociation of OPPh$_3$ and the formation of unidentified Mo complexes were observed upon standing. Similar results were reported by Seymore and Brown for a related Re system.[25] Furthermore, there was no IR evidence for significant isotope scrambling during the synthesis, isolation, and manipulation of [Tp$^{i\mathrm{Pr}}$Mo^{16}O(S*n*Bu)(^{18}OPEt$_3$)] from a mixture of [Tp$^{i\mathrm{Pr}}$Mo^{16}O(S*n*Bu)(NCMe)] and ^{18}OPEt$_3$. As stated above, the phosphoryl ligand is labile and is readily displaced by other ligands and coordinating solvents.

Phosphoryl complexes are well known and examples from group 6 chemistry span all common oxidation states and a wide range of coligands. Examples include [MO$_2$X$_2$(OPPh$_3$)$_2$], [MOCl$_3$(OPPh$_3$)$_2$] (M = Mo, W), [Mo$_2$O$_4$I$_2$(OPPh$_3$)$_3$], [Mo(NO)Cl$_3$(OPPh$_3$)], [CpMo(Me)X(OPPh$_3$)(NO)] (Cp = cyclopentadienyl, X = Cl, Br), *cis*-[Mo(CO)$_4$(OPR$_3$)$_2$], and *fac*-[Mo(CO)$_3$(OPPh$_3$)$_3$]; these and related species have been comprehensively reviewed.[26,27] Generally, they are prepared by treating a suitable precursor with the phosphine oxide; the title compounds are representive of the very few complexes that have been generated by direct attack of phosphines on oxo-Mo complexes.[12–14]

Characterization of the complexes: The oxo(phosphoryl) complexes were characterized by microanalytical, spectroscopic, mass spectrometric, and crystallographic techniques. Spectroscopic and mass spectrometric data are summarized in Table 1; full details may be found in the Supporting Information.

Infrared spectra exhibited conspicuous bands assignable to Tp$^{i\mathrm{Pr}}$ (ν(BH) ≈ 2470 cm^{-1} and ν(CN) ≈ 1510 cm^{-1}), terminal oxo (ν(Mo=O) = 966–943 cm^{-1}), and phosphoryl ligands (ν(P=O) = 1140–1083 cm^{-1}), as well as distinctive bands from the various coligands (for example, ν(C–O) ≈ 1590 cm^{-1} for phenolates). The ν(Mo=O) bands are in the region expected for monomeric oxomolybdenum(IV) species.[2,3] The ν(PO) band in the thiolate complexes was evident from spectral comparisons with the corresponding nitrile complexes and the observed shift from ν = 1096 cm^{-1} in [Tp$^{i\mathrm{Pr}}$MoO(S*n*Bu)(OPEt$_3$)] to ν = 1069 cm^{-1} in isotopically labeled [Tp$^{i\mathrm{Pr}}$MoO(S*n*Bu)(^{18}OPEt$_3$)]. The ν(PO) bands of the triethylphosphine oxide complexes were 70–80 cm^{-1} lower in energy than the corresponding band of the free ligand (ν = 1166 cm^{-1}),[28] in line with previously reported shifts of 10–100 cm^{-1} upon complexation.[26,29,30] It should be noted that some of the ν(PO) bands were broader than ex-

Table 1. Characterization data.

Compound no.: OPR_3, X	*m/z* $[M]^+$	IR (KBr): ν [cm^{-1}] (BH)	(MoO)	(PO)	^{1}H NMR in C_6D_6: δ [ppm] (multiplicity, no. of H) Tp^{iPr} methyl[a]	Tp^{iPr} methine[b]	Tp^{iPr} ring[c]	OPR_3[d]	X[e]	^{31}P NMR δ [ppm]
1: $OPEt_3$, Cl	622.2	2498, 2450	957	1095	1.08, 1.20, 1.29, 1.43, 1.44, 1.54	4.06, 4.16, 4.35	5.80, 6.02, 6.04, 7.28, 7.49, 7.62	0.84, 1.56, 2.16	–	78.8
2: $OPEt_3$, OPh	680.2	2477, 2450	950	1083	0.59, 1.00, 1.08, 1.19, 1.24, 1.68	2.65, 4.15, 4.42	5.86, 5.95, 6.00, 7.34, 7.42, 7.72	0.93, 1.68, 1.96	6.30 (2H), 6.68 (1H), 7.07 (2H)	78.8
3: $OPEt_3$, OC_6H_4-3-Me	694.4	2478, 2450	949	1094	0.60, 1.01, 1.09, 1.19, 1.25, 1.69	2.65, 4.16, 4.43	5.87, 5.96, 6.01, 7.36, 7.44, 7.73	0.95, 1.70, 1.97	2.13 (3H), 5.96 (1H), 6.20 (1H), 6.55 (1H), 7.02 (1H)	78.6
4: $OPEt_3$, OC_6H_4-3-*t*Bu	736.3	2483, 2448	950	1095	0.55, 1.02, 1.07, 1.19, 1.23, 1.67	2.62, 4.14, 4.15	5.88, 5.95, 5.99, 7.38, 7.43, 7.74	0.95, 1.70, 1.98	1.11 (9H), 6.03 (1H), 6.58, 6.79 (1H), 7.25 (2H)	78.9
5: $OPEt_3$, OC_6H_3-3,5-*t*Bu_2	792.4	2476, 2447	943	1088	0.51, 1.02, 1.02, 1.19, 1.23, 1.68	2.61, 4.14, 4.45	5.86, 5.95, 6.00, 7.38, 7.43, 7.75	0.99, 1.78, 1.99	1.35 (18H), 5.79, 6.70 (1H), 6.88 (1H)	78.5
6: $OPEt_3$, OC_6H_4-2-s*Bu*[*]	736.3	2474, 2445	945	1097	0.50, 0.55, 1.04, 1.04, 1.07, 1.07, 1.08, 1.09, 1.29, 1.33, 1.66, 1.68[*]	2.46, 4.15, 4.33	5.87, 5.88 (d, 2H′), 7.35, 7.43, 7.69 (d, 2H′)	0.93, 1.19, 1.26	1.6–1.8 (4H′), 3.31, 3.40 (1H), 5.69 (2H′), 5.94, 5.95 (2H), 6.6–6.8 (2H′)	78.1, 78.0
7: $OPEt_3$, S*n*Bu	676.5	2477, 2446	948	1096	1.11, 1.22, 1.35, 1.35, 1.51, 1.58	3.95, 4.10, 4.84	5.91, 5.96, 6.17, 7.32, 7.40, 7.70	0.88, 1.66, 2.22	0.83 (3H), 1.7–1.9 (2H), 2.23 (2H), 2.79 (2H)	79.6
8: $OPEt_3$, S*s*Bu*	676.5	2479, 2448	944	1093	0.61, 1.05, 1.28, 1.35, 1.59, 1.69[*]	2.99, 3.72, 4.22	5.88, 5.93, 6.18, 7.34, 7.72–7.74 (m, 2H)	0.91, 1.70, 2.25	1.25 (3H′), 1.51 (3H′), 1.90–2.08 (2H′), 4.52 (1H′)	79.0, 79.1
9: $OPMePh_2$, OPh	762.2	2480, 2451	948	1134	0.62, 0.67, 0.91, 0.93, 1.20, 1.51	2.86, 4.05, 4.07	5.85, 5.98, 6.03, 7.36, 7.46, 7.71	2.26 (3H), 6.98–7.22 (10H)	6.52 (2H) 7.00–6.73 (1H), 7.22 (2H)	55.0
10: $OPMePh_2$, OC_6H_4-3-Me	776.2	2478, 2450	952	1133	0.62, 0.69, 0.92, 0.94, 1.21, 1.52	2.88, 4.06, 4.06	5.86, 5.98, 6.03, 7.37, 7.47, 7.71	2.27 (3H), 6.99–7.22 (7H) 7.64–7.82 (3H)	2.18 (3H), 6.17 (1H), 6.43 (1H), 6.60 (1H)	54.1
11: $OPnBu_3$, OC_6H_4-4-Br	842.3	2473, 2445	950	1096	0.61, 1.04, 1.04, 1.16, 1.27, 1.67	2.53, 4.07, 4.35	5.82, 5.93, 5.99 7.32, 7.41, 7.68	0.86 (9H), 1.29 (6H), 1.42, 1.61 (3H), 1.80, 2.09 (3H)	6.04 (d, 2H), 7.12 (d, 2H)	74.7
12: $OPPh_3$, Cl	766.3	2485, 2453	966	1140	0.55 (6H), 1.24, 1.27, 1.42, 1.48	3.88, 4.09, 4.31	5.84, 6.03, 6.06 7.33, 7.54, 7.62	6.9–7.1, 7.9 (m)	–	51.6

[a] Doublet resonances integrating for 3H. (Note: there is some duplication in samples presenting isomeric forms (asterisked)). [b] Septet resonances integrating for 1H. (Note: there is some duplication in samples presenting isomeric forms). [c] Unless indicated, doublet resonances integrating for 1H. [d] For $OPEt_3$ complexes, the most shielded-resonance was a doublet of triplets (9H); the other two resonances were doublets of quartets (3H each) with $^3J_{H,P} \approx 17$, $^2J_{H,P} \approx 15$, and $^3J_{H,H} \approx 8$ Hz; see the Supporting Information for coupling details. [e] See the Supporting Information for coupling details.

pected or split to some extent by solid-state effects, which made assignments difficult; similar observations have been reported by Cotton et al.[31] Complex **11** exhibited a ν(PO) band at 1096 cm^{-1}, which is 73 cm^{-1} lower in energy than the corresponding band of $OPnBu_3$ (ν = 1169 cm^{-1}).[32] This is comparable to the 70 cm^{-1} spectral shift reported for $[MoO(O_2)_2(OPnBu_3)_2]$.[33] The ν(PO) bands of the $OPMePh_2$ and $OPPh_3$ complexes were approximately 60 cm^{-1} lower in energy than the free ligands (ν ≈ 1193 cm^{-1}),[34] in keeping with previous results.[29]

^{1}H NMR data (Table 1) confirmed the local C_1 symmetry of all species. For example, the spectrum of **3**, which is typical of these complexes, exhibited six doublet and three septet resonances assigned to the isopropyl groups of Tp^{iPr}, with the methine resonance at δ = 2.65 ppm being significantly shielded relative to others (δ > 4.16 ppm). Signals due to the ring protons of Tp^{iPr} were observed as two sets of three doublets. Singlet methyl and doublet (2×1H) and triplet (2×1H) aromatic resonances confirmed the presence of the 3-cresolate ligand. Complex resonances, distinctly different from those of free triethylphosphine oxide, characterized the coordinated phosphine oxide under local C_1 symmetry. For **3**, the diastereotopic methylene protons of the $OPEt_3$ were observed as two distinct doublet of doublet of quartet resonances at δ = 1.70 and 1.97 ppm (each 3H); an isopropyl methyl doublet partially obscured the δ = 1.70 ppm resonance in all but one of the complexes. Finally, a doublet of triplets at δ = 0.95 ppm was observed for the methyl protons of $OPEt_3$.

The NMR spectra obtained for complexes containing a chiral coligand were complicated by the presence of diastereomers, that is, (*R*,*R*)/(*S*,*S*) and (*R*,*S*)/(*S*,*R*) complexes, leading to an apparent duplication of resonances. Overlap in the ^{1}H NMR spectra prevented reliable integration but an accurate assessment of the isomer ratio was obtained from the well-separated ^{31}P NMR resonances of the enantiomeric pairs (see below). Variable-temperature NMR spectroscopy of **5** indicated the presence of restricted rotation about the phenolate O–C

bond in this sterically encumbered derivative, with broad room-temperature resonances transformed into sharper signals at higher temperatures.

$^{13}C\{^1H\}$ NMR spectra were collected for the more stable triethylphosphine oxide derivatives (see the Supporting Information). These exhibited doublet methyl ($\delta \approx 6.3$ ppm, $^2J_{C,P} \approx 4.5$ Hz) and methylene ($\delta \approx 19.0$ ppm, $^1J_{C,P} \approx 65$ Hz) phosphoryl resonances. The number of Tp^{iPr} and coligand resonances was concordant with expectations based on C_1 symmetry; for example, six methyl and three methine Tp^{iPr} resonances were observed.

$^{31}P\{^1H\}$ NMR spectra (Table 1) were consistent with the absence of phosphine oxide exchange in benzene on the NMR timescale. A single, sharp resonance was observed for all complexes except **6** and **8**, which exhibit two resonances ascribed to (*R*,*R*)/(*S*,*S*) and (*R*,*S*)/(*S*,*R*) enantiomeric pairs. Diastereomer ratios of 50:50 and 70:30 for **6** and **8** were determined by integration, although specific assignments were not persued. There was a clear chemical-shift dependence on the phosphine oxide, such that shielding increased in the order: $PEt_3 < PBu_3 < PMePh_2 < PPh_3$. The $OPEt_3$ complexes displayed resonances at $\delta = 78.0 \pm 1.5$ ppm, deshielded by approximately 26 ppm relative to free $OPEt_3$ ($\delta = 52.2$ ppm in C_6D_6), in line with literature reports.[26] ^{31}P chemical shifts were insensitive to the phenolate ligand and showed no correlation with coligand Hammett parameters. The resonances for **9**/**10**, **11**, and **12** were deshielded by 23–28 ppm relative to the free phosphine oxides (in $CDCl_3$, $\delta(OPMePh_2) = 28.7$, $\delta(OPnBu_3) = 46.9$, and $\delta(OPPh_3) = 29.3$ ppm[35]).

The spectroscopic properties of the acetonitrile and DMF complexes accorded with their formulations (see the Supporting Information). The IR spectra of the complexes exhibited bands due to Tp^{iPr} (ν(BH) = 2533–2481 cm^{-1}) and terminal oxo (ν(Mo=O) = 966–946 cm^{-1}) ligands. A nitrile ν(CN) mode was not observed but these are typically weak in intensity.[30] Coordinated DMF was revealed by a ν(C=O) band at 1645 cm^{-1} (compared with $\nu = 1671$ cm^{-1} for free DMF).[30] The ^1H NMR spectrum of freshly prepared solutions revealed resonances consistent with C_1 symmetry and the presence of acetonitrile ($\delta = 3.06$ ppm) or DMF ($\delta = 2.95$ and 2.80 ppm (methyl groups), $\delta = 8.03$ ppm (C(O)H)) ligands. Exchange of the coordinated and deuterated solvents was evident with time. Mass spectrometry of the complexes dissolved in acetonitrile confirmed the mononuclear formulation. For [Tp^{iPr}MoO(S*n*Bu)(DMF)], a parent ion for [Tp^{iPr}MoO(S*n*Bu)(NCMe)] (*m*/*z* 583.2) was observed due to rapid ligand exchange in the sample.

Crystallographic studies: The crystal structures of compounds **6**, **7**, **9**, and **12** were determined by X-ray diffraction. The molecular structures are displayed in Figures 1–4, and selected metrical data are presented in Table 2. These structures complement the published structure of **2**,[12] the data for which are included for comparison and completeness in Table 2 and the following discussion. All five complexes exhibit distorted octahedral Mo centers complexed by a tri-

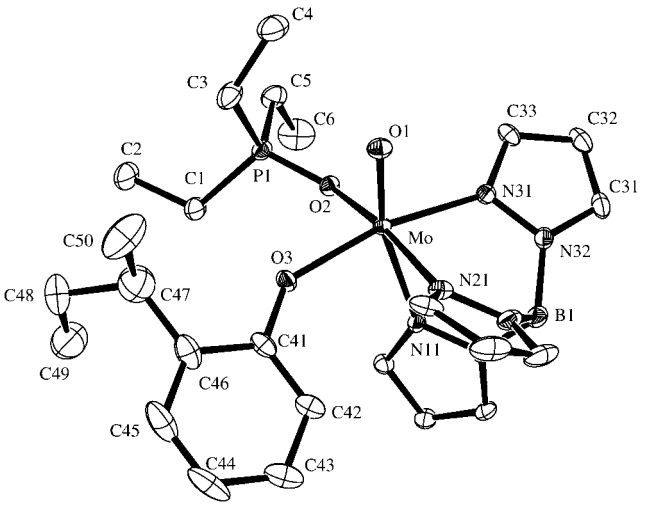

Figure 1. Molecular structure of **6**. The numbering schemes for the pyrazole rings containing N11 and N21 follow that shown for the ring containing N31. The Tp^{iPr} isopropyl groups and hydrogen atoms have been removed for clarity and probability ellipsoids are shown at the 30% level.

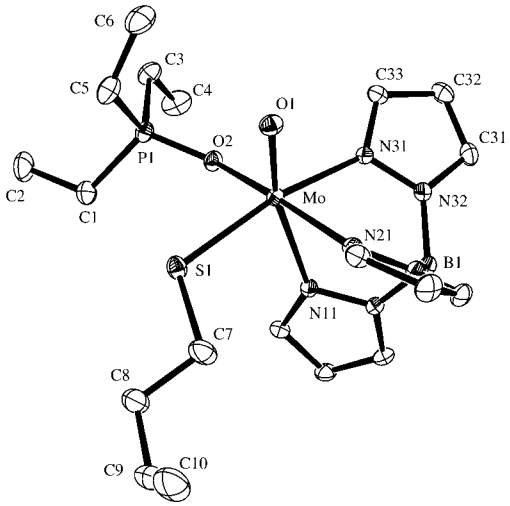

Figure 2. Molecular structure of **7**. See the legend of Figure 1 for further details.

dentate *fac*-Tp^{iPr} ligand and mutually *cis* terminal oxo, phosphine oxide, and phenolate or thiolate ligands.

We begin our discussion with the triethylphosphine oxide complexes. Here, the Mo=O bond lengths lie in the range 1.682(2)–1.6913(15) Å, in the region typical of oxomolybdenum(IV) species.[36,37] The Mo–O3 and Mo–S1 distances of approximately 2.034 and 2.3930(6) Å are within the ranges expected for phenolate and thiolate ligands to Mo.[37] The Mo–OP and O–P distances fall in the ranges 2.157(3)–2.1706(14) and 1.511(2)–1.5189(15) Å, respectively; the former are typical of Mo–OPR_3 complexes.[37] The P–O distances are not significantly different from those observed for lattice $OPEt_3$ in $[Mo_3(\mu_3\text{-}S)(\mu\text{-}S)_3Cl_4(PEt_3)_3(H_2O)_2]\cdot OPEt_3$ (1.511(7) Å)[38] and $[PtI\{OPEt_3\}\{P(OH)Et_2\}_2]\cdot OPEt_3$

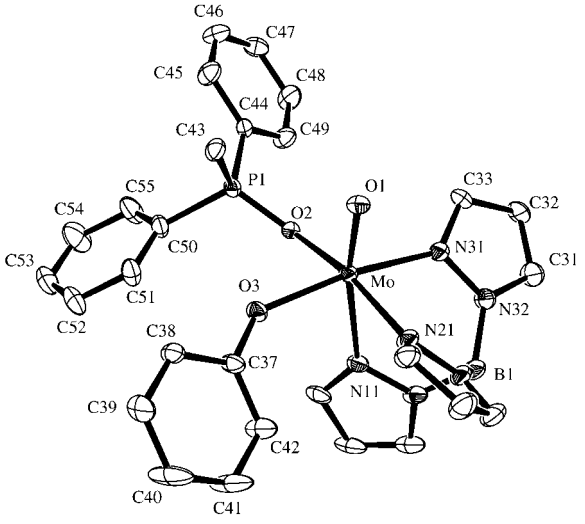

Figure 3. Molecular structure of **9**. See the legend of Figure 1 for further details.

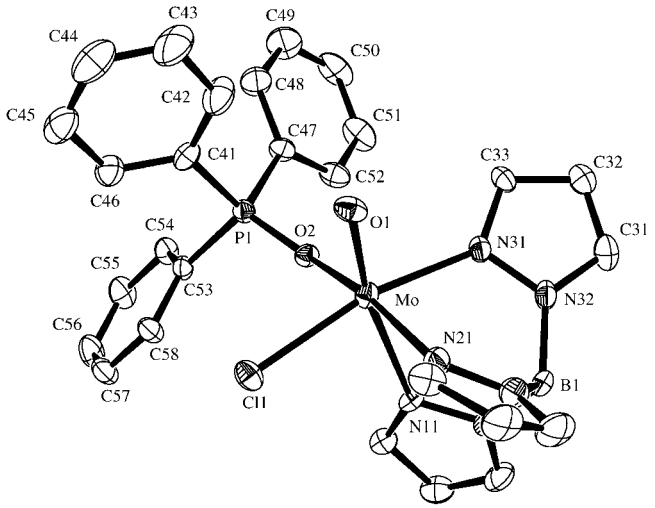

Figure 4. Molecular structure of **12**. See the legend of Figure 1 for further details.

(1.499(4) Å),[39] consistent with the presence of multiple bonding. The P–O bond lengths are substantially shorter than a P–O single bond (1.60 Å), as is present in P_4O_{10}, etc.[40] The complexes are very similar in their triethylphosphine oxide and coligand (X) conformations, as dictated by the steric constraints of the Tp^{iPr} ligand (see below). When the Mo(=O)N_3 portions of the three molecules are superimposed, the Mo–O–P fragments are closely coincident with spatial separations of less than 0.21 and 0.47 Å for the O and P atoms, respectively (see Figure 5 for superposition of *all* structures except (for clarity) **12**). There is considerable congruence of the Mo-O-P angles (130.9(2)–135.57(9)°) and O=Mo-O-P torsion angles (52.6(4)°–57.5(3)°); the smallest Mo-O-P and largest O=Mo-O-P angles are associated with the least hindered of the complexes (**2**). The bent Mo-O-P units are consistent with the use of π electron density in the bonding of the phosphine oxide to the metal. The ethyl substituents also occupy similar regions, the Mo-O-P-C torsion angles spanning a range of only 10°. The phenolate rings in **2** and **6** lie in the same plane, with a small displacement (max. 0.39 Å) due to a difference in the Mo-O3-C angles. In all cases, the coligand substituent projects away from the Tp^{iPr} ligand, with the *sec*-butyl group in **6** being directed away from the sterically restricted cleft between the Tp^{iPr} pyrazolyl groups. The steric clash of the *sec*-butyl and ethyl groups on neighboring ligands appears to be responsible for observed differences. The butyl substituent of **7** zigzags through the same region of space occupied by the phenolate rings in the other structures.

The Mo–N(n1) (n = 1–3) distances are in accord with expectations based on the *trans* influence of the various coligands, that is, =O > X > $OPEt_3$. In each case, the Mo atom sits out of the equatorial plane defined by N21, N31, O2, and O3/S1, toward the terminal oxo ligand, by approximately 0.28 Å. The greatest angular deviations from ideal octahedral geometry are seen in the O1-Mo-O2, O1-Mo-E (E = O, S), and O1-Mo-N11 angles, which lie in the ranges 97.3(1)–98.54(7)°, 104.67(6)–108.89(10)°, and 164.8(1)–166.66(7)°, respectively.

Very few triethylphosphine oxide complexes have been structurally characterized. Previous examples from molybdenum chemistry are limited to the dinuclear species $[Mo_2(S_2CPEt_3)(O_2CCH_3)_3(OPEt_3)]BF_4$ (Mo–O 2.348(5) Å, P–O 1.502(5) Å, Mo–O–P 145°)[41] and $[MoCl(NO)_2(OPEt_3)]_2(\mu\text{-}Cl)$ (Mo–O 2.091(2) Å, P–O 1.517(2) Å, Mo–O–P 145.3(1)°).[42] The source of the phosphine oxide in both compounds remains unclear. The present complexes represent the first structurally characterized examples of monomeric oxo(triethylphosphine oxide)molybdenum complexes and the first complexes of this type to be generated by incomplete OAT.

For **9**, the terminal oxo ligand is bound at a distance of 1.684(3) Å, while the phenolate exhibits an Mo–O bond length (2.027(3) Å) typical of Mo–OAr bonds. The phosphoryl ligand is coordinated at an Mo–O2 distance of 2.172(3) Å, with an O–P bond length of 1.512(3) Å. These compare to the analogous distances of 2.100 Å (av Mo–O) and 1.495 Å (av O–P) in $[MoOCl_3(OPMePh_2)_2]\cdot C_6H_6$, the only other structurally characterized $OPMePh_2$ complex of Mo.[43] The O=Mo-O-P torsion angle of 46.8(3)° is slightly smaller than in the other structures. The orientations and conformations of the ligands are generally similar to the triethylphosphine oxide complexes above, with the superpositions of **2** and **9** indicating displacements of only 0.18 and 0.24 Å for the O(P) and P atoms, respectively (see Figure 5). The steric interaction of phenyl groups on the $OPMePh_2$ and OPh ligands results in a small tilting of the OPh group of **9** away from the position occupied in **2** (a dihedral angle of approximately 8° relates the two phenyl planes, hinged at a common O–Ar site (ΔO = 0.07 Å). The Mo-O-P and O=Mo-O-P torsion angles are 131.91(19)° and 46.8(3)°, respectively.

Table 2. Metrical parameters.

Parameter[a]	2[b]	6	7	9	12
Mo–O1	1.684(3)	1.682(2)	1.6913(15)	1.684(3)	1.748(5)
Mo–O2	2.157(3)	2.168(2)	2.1706(14)	2.172(3)	2.159(4)
Mo–E	2.031(3)	2.036(2)	2.3930(6)	2.027(3)	2.397(2)
Mo–N11	2.430(4)	2.377(2)	2.4554(17)	2.412(4)	2.411(6)
Mo–N21	2.155(4)	2.150(3)	2.1786(17)	2.147(4)	2.161(6)
Mo–N31	2.212(4)	2.199(2)	2.2421(18)	2.193(4)	2.205(6)
O2–P1	1.516(3)	1.511(2)	1.5189(15)	1.512(3)	1.498(4)
O1-Mo-O2	97.3(1)	98.08(9)	98.54(7)	99.00(14)	98.5(2)
O1-Mo-E	108.0(2)	108.89(10)	104.67(6)	105.14(15)	102.07(17)
O1-Mo-N11	164.8(1)	165.21(9)	166.66(7)	168.35(15)	169.7(2)
O1-Mo-N21	91.3(2)	92.95(10)	90.27(7)	93.58(16)	93.2(2)
O1-Mo-N31	90.0(2)	90.02(10)	91.91(7)	90.92(15)	92.2(2)
O2-Mo-E	79.1(1)	81.72(8)	85.78(4)	80.07(12)	85.69(13)
O2-Mo-N11	91.7(1)	87.25(8)	87.86(6)	85.57(13)	86.91(18)
O2-Mo-N21	171.2(1)	168.97(8)	170.10(6)	167.42(14)	168.2(2)
O2-Mo-N31	93.7(1)	91.42(8)	88.77(6)	92.84(13)	93.4(2)
E-Mo-N11	85.7(1)	85.47(8)	87.39(4)	86.15(13)	86.96(5)
E-Mo-N21	96.8(1)	94.93(9)	96.39(5)	96.72(14)	91.18(18)
E-Mo-N31	161.2(1)	160.55(9)	163.14(5)	163.23(14)	165.96(17)
N11-Mo-N21	80.2(1)	82.00(9)	82.61(6)	82.07(15)	81.6(2)
N11-Mo-N31	77.2(1)	76.00(9)	76.46(6)	78.11(14)	78.7(2)
N21-Mo-N31	87.9(1)	88.36(10)	86.42(7)	86.91(14)	86.8(2)
Mo-O2-P1	130.9(2)	133.52(12)	135.57(9)	131.91(19)	146.7(3)
O1-Mo-O2-P1	−57.5(3)	−53.5(2)	−52.6(4)	−46.8(3)	−33.1(5)
O1-Mo-E-C	−103.4(4)	−108.9(3)	−111.5(4)	−99.1(4)	–

[a] E = O3 for **6** and **9**, S1 for **7**, and Cl1 for **12**. [b] Data for **2** were taken from reference [12]. A modified numbering scheme has been adopted to make the data directly comparable, that is, atom numbers O2/O3 and N21/N31 in ref. [12] have been exchanged.

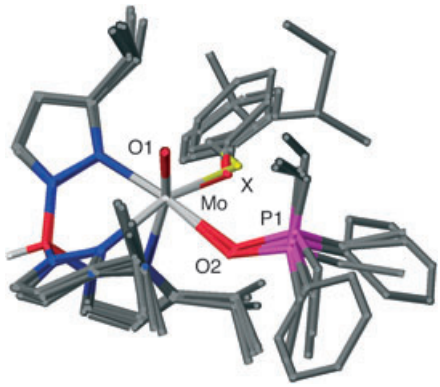

Figure 5. Superposition of the structures of **2**, **6**, **7**, and **9** showing congruence of the Tp^{iPr} isopropyl, OPR_3, and X groups.

In **12**, the steric bulk of the triphenylphosphine oxide results in a considerably greater displacement of 0.66 Å between P atom sites of superimposed molecules of **2** and **12**; the corresponding displacement in the O(P) sites remains small (0.17 Å). The Mo-O-P angle of 146.7(3)° is considerably opened relative to the other derivatives and the O=Mo-O-P torsion angle of 33.1(5)° is the smallest observed for the series of structurally characterized compounds. The P–O distance of 1.498(4) Å is not significantly different from the values determined for orthorhombic (1.491 Å) and monoclinic (1.494 Å) forms of $OPPh_3$ at 100 K.[44] Nevertheless, the phenyl substituents adopt the broad conformations observed for the earlier complexes. The chloride ligand is sited close to the midpoint of the O–C(Ar) bond of the superimposed molecule **2**, with the Mo–Cl1 distance being 2.397(2) Å.

Electronic structures: The electronic structures of the crystallographically characterized complexes were probed by using density functional theory (DFT). The atomic orbital contributions of selected molecular orbitals are summarized in Table 3. As expected, the ligand field was dominated by the terminal oxo ligand and the metal orbital manifolds were organized accordingly (Figure 6). In each case, the molybdenum $4d_{xy}$ orbital was the major contributor to the highest occupied molecular orbital (HOMO; see, for example, Figure 7 and Table 3). Interestingly, the energies of the HOMOs were nearly invariant to the nature of the equatorial phosphoryl ligands, the energy range of the HOMOs being 0.171 eV (Table 3) and the ligand orbital contributions practically constant. However, the contribution from the equatorial ligand X to the HOMO (primarily through a pseudo-π bonding interaction) varied from 4.8% in **9** to 8.8% in **7**. The nature of the donor atom alone cannot explain this difference. For instance, the contributions of X to the HOMOs of **2** and **6** (4.9 and 7.5%, respectively) differ significantly despite the phenolate character of both X groups. However, at a qualitative level, these differences can be explained on the basis of the O=Mo-E-C torsion angles. It has been proposed that for $[MoO_2(SMe)(S_2C_2Me_2)]^-$, the O-Mo-S-C torsion angle can modulate the percent contribution from the equatorial SMe ligand to the lowest unoccupied molecular orbital (LUMO; predominantly d_{xy}) in a sinusoidal manner.[45] In the title complexes the overall behavior is similar: the larger the O=Mo-E-C torsion angle, the larger the contribution of the ER equatorial ligand to the predominantly d_{xy} molecular orbital. In all cases, except **9** and **12**, the LUMO and LUMO+1 orbitals predominantly consist of the d_{xz} and d_{yz} metal-centered atomic orbitals, respectively. In the case of complex **12**, the d_{yz} orbital was delocalized between the LUMO+1 and the LUMO+2 orbitals (Table 3). On the other hand, two molecular orbitals, primarily composed of phenyl π* orbitals of the $OPPh_2Me$ ligand, were located in between the HOMO and the d_{xz} orbital of **9** (see the Supporting Information). The calculated d_{xy} to d_{xz} energy difference for **12** was 2.725 eV, but this dif-

Table 3. Calculated energies and compositions of selected molecular orbitals.

Orbital	Compound	OPR_3	X	E [eV]	Orbital composition [%]				
					Mo	O_t	X	OPR_3	Tp^{iPr}
d_{xy}	**2**	$OPEt_3$	OPh	−4.247	83.6	0.3	4.9	3.7	7.4
	6	$OPEt_3$	OC_6H_4sBu	−4.193	81.5	0.4	7.5	3.2	7.4
	7	$OPEt_3$	S*n*Bu	−4.269	80.0	0.6	8.8	3.1	7.4
	9	$OPMePh_2$	OPh	−4.167	82.8	0.3	4.8	4.6	7.5
	12	$OPPh_3$	Cl	−4.338	80.4	0.3	6.8	5.1	7.3
d_{xz}	**2**	$OPEt_3$	OPh	−1.199	62.8	13.7	3.3	9.3	13.7
	6	$OPEt_3$	OC_6H_4sBu	−1.182	60.7	10.9	3.0	9.3	16.2
	7	$OPEt_3$	S*n*Bu	−1.187	65.5	11.4	1.0	9.1	12.9
	9	$OPMePh_2$	OPh	−1.115	51.7	9.1	1.9	24.8	12.5
	12	$OPPh_3$	Cl	−1.613	51.7	8.7	0.5	31.1	8.0
d_{yz}	**2**	$OPEt_3$	OPh	−0.750	62.8	10.0	6.7	1.8	18.7
	6	$OPEt_3$	OC_6H_4sBu	−0.689	60.3	9.5	7.0	1.9	21.4
	7	$OPEt_3$	S*n*Bu	−0.860	61.7	9.5	9.3	2.0	17.6
	9	$OPMePh_2$	OPh	−0.758	61.7	9.9	7.2	2.4	18.7
	12[a]	$OPPh_3$	Cl	−1.443	34.4	5.4	2.1	50.8	7.4
	12[a]	$OPPh_3$	Cl	−1.395	48.6	7.9	2.8	30.0	10.7

[a] The d_{yz} orbital of **12** is delocalized between the LUMO and LUMO+1 orbitals.

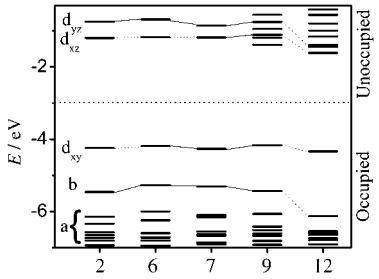

Figure 6. Molecular orbital diagrams for selected compounds. Details of the DFT calculations can be found in the text.

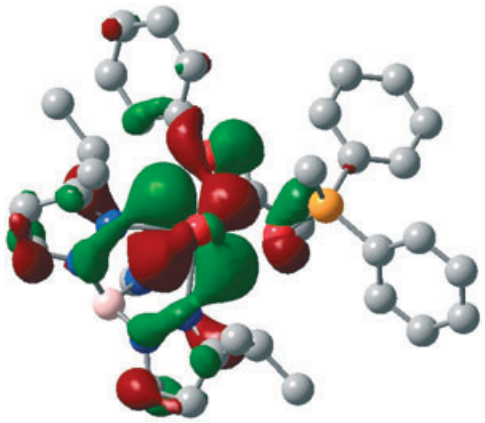

Figure 7. Model of the HOMO for **9**. The calculated HOMOs for all complexes are very similar to the example presented.

ference was slightly higher and nearly constant for the other complexes (3.011–3.082 eV). Again, the energy differences between the d_{xz} and d_{yz} orbitals (with the exception of **12**) were nearly constant (0.327–0.493 eV; Table 3). Consistent with this description of the energy levels, a low-energy band at ≈890 nm, attributed to the $d_{xy}\rightarrow d_{xz}$ transition, was observed. A shoulder, presumably due to the $d_{xy}\rightarrow d_{yz}$ transition, could also be located in the higher energy region in the optical spectra of **2** and **9**.[19] The differences in energy between these two bands were ≈0.402 and 0.441 eV, respectively, with the computed values being 0.449 and 0.357 eV.

The $d_{x^2-y^2}$ and d_{z^2} metal-centered orbitals are highly delocalized over a few molecular orbitals (Tables S1–S5 in the Supporting Information). In general, the relative order of the molecular orbitals was approximately the same: $OPR_3(\pi) < Tp^{iPr}(\pi) \approx ER(\pi) < d_{xy}(HOMO) < d_{xz} < d_{yz} < Tp^{iPr}$, OPR_3 ($\pi*$). In all cases the low-lying π-acceptor orbitals were found to be located on the tris(pyrazolyl)borate[46,47] and OPR_3 ligands.

Stability of the complexes: The computational study of *sterically unencumbered* $[MoO(OPMe_3)(SH)_2(NH_3)_2]$ by Hall and co-workers determined an O=Mo-O-P torsion angle close to 0° for the complex.[17] In contrast, the O=Mo-O-P torsion angles of the title complexes lie in the range 47–59°. To understand the underlying reasons for this difference, we have calculated 3D energy surfaces at the PM3(tm) semiempirical level for all of the structurally characterized complexes. The results are summarized in Figure 8 and in Figures S1 and S2 (see the Supporting Information). The figures show that the energy of a specific conformer is primarily controlled by the *steric* interactions between the equatorial phosphine oxide and the Tp^{iPr} and X ligands. The shape of the steric binding pocket is dominated by the conformational flexibility of the OPR_3 ligand. For example, in the $OPEt_3$

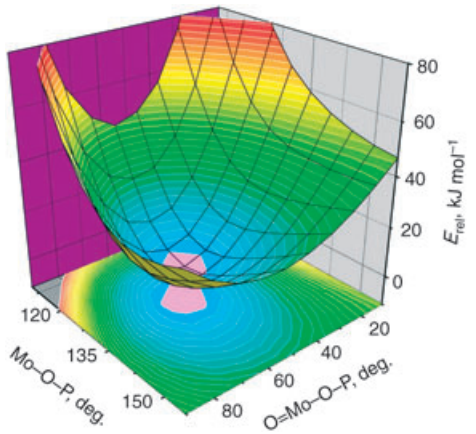

Figure 8. Three-dimensional energy surface of **7** as a function of phosphine conformation, as calculated by semiempirical methods. See the text for details.

complexes the shape of the binding pocket is nearly symmetrical, while the shapes of those of the $OPPh_2Me$ and $OPPh_3$ complexes are not. A closer look at the surfaces suggests that at room temperature (298 K), where the thermal energy, kT (k = Boltzmann constant, T = absolute temperature), is equivalent to approximately 2.5 kJ mol^{-1}, the rotational freedom of the phosphoryl ligand is constrained to a small range of Mo-O-P and O=Mo-O-P torsion angles. This smaller area results in a more restricted rotation for the aryl phosphoryl ligands.

It is interesting to compare the area (designated as the rotation area) where the phosphine oxide can rotate freely at room temperature for the different complexes. Qualitatively, the rotation area of **2** is about 1.7 times larger than that of **6**, a fact suggesting that the *sec*-butyl group contributes to the restricted rotation of the phosphoryl ligand. Similarly, the rotation area of **9** is significantly smaller ($\approx$5 times) than that of **2**. This is consistent with the kinetic experiments conducted in our laboratories, in which **9** decays approximately five times faster than **2** at 5 °C. Although details of the mechanistic studies will be presented elsewhere,[19] a few important aspects are worthy of discussion here. There are two major contributions to the molybdenum–phosphine oxide interaction in these complexes, electronic and steric. The basicity of the tertiary phosphine oxides is lower compared to related amine oxides. For instance, the pK_b value for Me_3N=O is 9.3,[48] while pK_b values for trialkylphosphine oxides approach 15.5.[49] Moreover, the basicities of the phosphine oxides fall in a very narrow range: $\approx$15.5 for trialkylphosphine oxides, 16.4 for $OPMe_2Ph$, and 17.0 for $OPPh_3$.[48,49] This behavior is significantly different from that of tertiary phosphines, where large differences in basicity lead to a large difference in the metal–phosphine interactions. Thus, in a first approximation, the electronic contribution to the Mo–OPR_3 interaction is nearly constant. The steric contribution to the metal–phosphine interaction, as defined by Tolman,[50] has been discussed extensively in the literature. In the case of the complexes under discussion, it is the phosphine oxides that coordinate to Mo rather than the terminal oxo group to the phosphine (based on observed Mo–O and O=P distances). The net effect is that the steric interactions in these complexes originate from the cone angle of the OPR_3 ligand and the steric properties of the Tp$^{i\mathrm{Pr}}$ and X ligands. By using the crystallographic approach of Miller and Mingos,[51] the following cone angles have been determined for the phosphoryl ligands in the title complexes: For $OPEt_3$, 119.1° (**2**), 114.6° (**6**), 114.1° (**7**); for $OPMePh_2$, 122.7° (**9**); and for $OPPh_3$, 122.7° (**12**). In the case of the X ligands, the steric influence follows the order: OC_6H_4-2-*s*Bu > OPh $\approx$ S*n*Bu > Cl. On the other hand, the steric influence for the tripodal Tp$^{i\mathrm{Pr}}$ ligand (defined as a plane between three CH protons of the *i*Pr groups) is nearly constant for all complexes (minimal area is 7.59 Å^2 for **6** and maximum area is 8.06 Å^2 for **7**). When all this information is taken into consideration, it is expected that the "kT" area should follow the order **7** $\approx$ **2** > **6** > **9**, which is in excellent agreement with the PM3(tm)-generated 3D surfaces (Figure 8 and Figures S1 and S2 in the Supporting Information). Despite a larger estimated cone angle for $OPPh_3$ than $OPEt_3$, the calculated "kT" area for **12** is larger than that for **2** and **7**. This unexpected observation can be attributed to a difference in the steric properties of the OPh and S*n*Bu equatorial ligands in **2** and **7**, respectively, as compared to the Cl ligand in **12**. To test this hypothesis, we have calculated the 3D potential surface of a hypothetical complex, [Tp$^{i\mathrm{Pr}}$MoO(OPh)($OPPh_3$)] (**13**), the geometry of which was constructed by using the known geometries of **2** and **9**, but with $OPPh_3$ as the phosphine oxide. Based on the estimated cone angles of OPR_3 ligands, the expected "kT" areas follow the order **2** > **9** $\approx$ **13**, but the calculated "kT" areas follow the order **2** > **13** > **9**. Such a deviation can be explained only if the *conformational flexibility* of the PR_3 fragment in the OPR_3 ligand is taken into consideration. Detailed analysis of all of the available crystal structures with PR_3 ligands suggests that the conformational flexibility of the PR_3 ligands decreases in the order: PPh_3 (39.3°) > PEt_3 (35.8°) > $PMePh_2$ (32.3°).[51] It was suggested that the large conformational flexibility of the PPh_3 ligand can also modulate the M-P-C angle and the dihedral angle between the phenyl plane and the M-P-C plane.[51] Such rotational freedom of the phenyl ring is restricted in the $OPMePh_2$ ligand by the rigid methyl group. When this information is taken together, the expected "kT" area should follow the order **2** > **13** > **9**, which is in excellent agreement with the PM3(tm)-generated 3D potential surfaces.

Another interesting observation is that the minimum energy for each O=Mo-O-P torsion angle has a different Mo-O-P angle. In other words, the energy of [Tp$^{i\mathrm{Pr}}$MoOX(OPR_3)] complexes depends not only on the O=Mo-O-P torsion angle but also on the Mo-O-P angle. When the relative energies of the lowest energy conformers were plotted against the O=Mo-O-P torsion angle, a nonsymmetric (with respect to the torsion angle) behavior was observed (Figure 9). All traces went through a minimum of approximately 55°, in agreement with experimental data. The left side of the graph, with dihedral angles of 10–55°, represents the steric interaction between the phosphoryl and trispyrazolylborate ligands, while the right side with dihedral angles

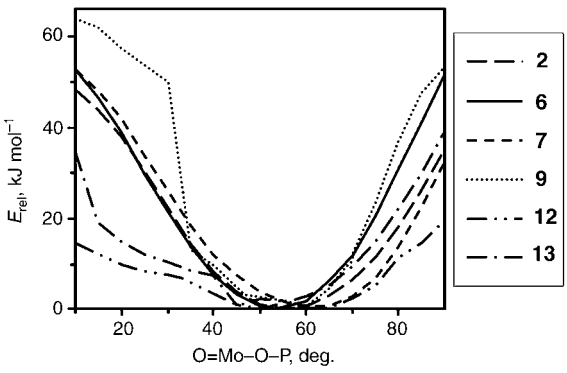

Figure 9. Calculated energy response as a function of the O=Mo-O-P torsion angle. Data points have been removed for clarity.

of 55–90° represents the steric interaction between the phosphoryl, Tp^{iPr}, and X ligands. The interaction between the phosphoryl and Tp^{iPr} ligands follows a similar pattern in all complexes except for **9** and **12**, a fact lending support to the idea that, in this region, the dominating interaction is the interaction between the phosphoryl and Tp^{iPr} ligands. Such interactions can only be increased with bulkier groups in the trispyrazolylborate fragment or in the OPR_3 ligand as seen in **9**. On the other hand, conformational flexibility of the PPh_3 group leads to a reduction of these steric interactions.

As mentioned, for O=Mo-O-P torsion angles greater than 55°, the *i*Pr group of Tp^{iPr} and X interact with the OPR_3 group and, as a result, the energy profiles are quite different for different compounds (Figure 9). Thus, the energy profile of **6** deviates significantly, by 8–16 kJ mol^{-1}, from those of the sterically less crowded **2** and **7**. The low-energy barrier for **12** originates from the smaller equatorial chloro ligand, while the hypothetical **13** shows an energy profile that is similar to complexes **2** and **7**. Interestingly, the steric interactions caused by the $OPMePh_2$ ligand are quite comparable to those of the *sec*-butyl group in the coligand of **6**. Finally, we note that the calculated 3D surfaces of the complexes agree well with X-ray data. Thus, the PM3(tm) method provides reliable relative energies of transition-metal complexes, as noted by others. In the earlier, simplified computational model,[17] the small steric requirement can lead to an energetically favorable conformation with an O=Mo-O-P torsion angle close to 0°.

In the crystal structures of several mononuclear molybdenum enzymes, for example, sulfite oxidase and DMSO reductases, the Mo center was found to be deeply buried inside the protein matrix, often at the bottom of a cavity or crevice, with the catalytic pockets tightly defined by the nearby amino acid residues and the cofactor.[52] While the "energy-controlled pockets" discussed here may differ in their exact nature, the pocket may play a role in defining the mechanism of the product dissociation. Thus, it is provocative to speculate as to how steric interactions can influence the mechanism of the product dissociation in this system. Due to the restrictive nature of the energy-controlled pockets, the formation of a solvated product with higher coordination number can be inhibited, thereby favoring the dissociation of the coordinated phosphine oxide first. Indeed, on-going studies in our laboratories suggest that dissociation of phosphine oxide from **2** and **9** proceeds through a dissociative interchange mechanism; results from these studies will be communicated in a forthcoming paper.[19]

Summary

Reaction of dioxomolybdenum(VI) complexes with phosphines leads to the formation of the oxo(phosphoryl)molybdenum(IV) complexes $[Tp^{iPr}Mo^{IV}OX(OPR_3)]$ by incomplete OAT from Mo^{VI} to P^{III}. The complexes, which are intermediates along the OAT reaction coordinate, represent rare examples of "substrate-bound" species isolated in molybdenum-enzyme model studies. Their isolation and structural, theoretical, and kinetic[19] evaluation constitute significant advances in the study of metal-mediated OAT reactions by high-valent oxo transition-metal complexes.

A comparison of structure parameters obtained by X-ray crystallography and theoretical studies (reference [17] and herein) reveals good agreement between experiment and theory. However, the intermediate identified in an earlier computational study examining OAT from $[MoO_2(SH)_2(NH_3)_2]$ with PMe_3, that is, $[MoO(SH)_2(NH_3)_2(OPMe_3)]$, exhibits a markedly different O=Mo-O-P torsion angle (approximately 0°) to those of the title complexes (approximately 50°). Eclipse of the oxo and phosphoryl multiple bonds of $[Mo(=O)(SH)_2(NH_3)_2(O=PMe_3)]$ is proposed to cause complete disruption of Mo–OP π bonding, thereby facilitating solvent-assisted dissociation of phosphine oxide. The torsion angles observed in the title complexes are dictated by steric interactions between the Tp^{iPr}, coligand X, and phosphine substituents R, with the PR_3 group residing in an energy-controlled binding pocket that induces a torsion angle of 50°. Restricted rotation about the Mo–O bond appears to maintain sufficient Mo–O π bonding to confer stability and isolability on the title complexes. Detailed kinetics studies of the reactions of $[Tp^{iPr}MoO_2(OPh)]$ with PEt_3 and $PMePh_2$ and the solvent-assisted decomplexation of phosphine oxide from **2** and **9**, along with a complete theoretical assessment of these reactions will appear in a forthcoming paper.[19]

Experimental Section

Materials and methods: The precursor compounds, $[Tp^{iPr}MoO_2X]$, were prepared by literature methods.[20] All reactions and workup procedures were performed under an atmosphere of pure dinitrogen by employing standard Schlenk techniques. All solvents were carefully dried and deoxygenated before use. Samples of $^{18}OPEt_3$ ($\nu(^{18}O=P) = 1106$ cm^{-1} (compare with $\nu = 1139$ cm^{-1} in $^{16}OPEt_3$), $\delta(^{31}P) = 52.2$ ppm in benzene (compare with $\delta(^{31}P) = 48.3$ ppm for $^{16}OPEt_3$ in CS_2)[53]) were prepared by adapting the method described for the preparation of $^{18}OPPh_3$ by Mayer and co-workers.[54]

Infrared spectra were recorded on a Biorad FTS 165 FTIR spectrophotometer as pressed KBr disks. NMR spectra were obtained by using Varian FT Unity 300 or INOVA400WB spectrometers and were referenced to tetramethylsilane or external H_3PO_4 ($\delta = 0$ ppm). UV/Vis spectra were recorded on Hitachi 150–20 or Shimadzu UV-2401PC spectrophotometers. X-Band EPR spectra were recorded at ambient temperature on a Bruker ECS 106 EPR spectrometer using 1,2-diphenyl-2-picrylhydrazyl as reference. Mass spectra were conducted with a Bruker BioApex 47e FTMS spectrometer fitted with an Analytica electrospray source operating with capillary voltages between 50–120 V; compounds were diluted with CH_2Cl_2 or MeCN and run immediately. Microanalyses were obtained from Atlantic Microlab, Inc., GA, USA. Spectroscopic and mass spectrometric data are summarized in Table 1. Full listings of analytical and spectroscopic data are included in the Supporting Information.

Preparation of $[Tp^{iPr}MoOCl(OPR_3)]$ complexes: A yellow solution of $[Tp^{iPr}MoO_2Cl]$ (200 mg, 0.4 mmol) in dry benzene (10 mL) was treated with PR_3 (1.5 equivalents) and the resultant green (R = Et) or brown (R = Ph) solution was stirred for 5 h. The solvent was removed in vacuo and dry hexane (10 mL) was added to the residue. Cooling to −4 °C produced green (R = Et) or beige (R = Ph) crystals, which were collected by

filtration, washed with hexane, and dried in vacuo. Yields were typically 50–60%.

Preparation of [Tp^{iPr}MoO(OAr)(OPEt$_3$)] complexes: The synthesis of **3** described here is typical. A solution of [Tp^{iPr}MoO$_2$(OC$_6$H$_4$-3-Me)] (288 mg, 0.5 mmol) in dry benzene, toluene, or MeCN (10 mL) was treated with PEt$_3$ (110 μL, 0.75 mmol) and then stirred at room temperature for 24 h. During this time the solution darkened to a golden-brown (toluene, benzene) or emerald-green (MeCN) color. The solvent was removed in vacuo and the residue was triturated with dry hexane (10 mL); this process was repeated in order to remove all MeCN. Cooling to −4 °C produced green crystals, which were collected by filtration, washed with hexane, and dried in vacuo. The yield was 230 mg (70%) for **3** and was typically in the range 50–75% for other derivatives.

Preparation of [Tp^{iPr}MoO(SR)(OPEt$_3$)] (R = *n*Bu, *s*Bu) complexes:

Method A: A solution of [Tp^{iPr}MoO$_2$(SR)] (212 mg, 0.38 mmol) in dry MeCN (10 mL) was treated with PEt$_3$ (84 μL, 0.57 mmol) and stirred for 24 h. The solvent was evaporated and the residue was treated with dry hexane (15 mL) and stirred for 1 h to produce a light-blue suspension. The evaporation and hexane treatment above were repeated two more times. The final green solution was filtered and the filtrate was reduced in volume (to approximately 5–10 mL) and cooled to −4 °C. The resulting green crystals were filtered in air, washed with small amounts of cold hexane, and dried in vacuo. The yields were approximately 105 mg (40%).

Method B: A solution of [Tp^{iPr}MoO$_2$(SR)] (212 mg, 0.38 mmol) in dry benzene or toluene (10 mL) was treated with PEt$_3$ (84 μL, 0.57 mmol) and the solution was stirred for 24 h. The solvent was evaporated and the residue was treated with dry hexane (10 mL) with stirring. Cooling of the solution to −4 °C produced green crystals, which were filtered, washed with hexane, and dried in vacuo. The yields were approximately 210 mg (80%).

Method C: A solution of [Tp^{iPr}MoO(SR)(MeCN)] (150 mg, 0.26 mmol) in dry acetonitrile or hexane (10 mL) was *immediately* treated with OPEt$_3$ (57 μL, 0.39 mmol) and the solution was stirred for 1 h. The workup procedure in Method A was followed to yield a green solid. The yields were 30–50%.

Preparation of [Tp^{iPr}MoO(OAr)(OPMePh$_2$)] complexes: The procedure described here for **9** is generally applicable. A solution of [Tp^{iPr}MoO$_2$(OPh)] (252 mg, 0.45 mmol) in dry benzene, toluene, or MeCN (10 mL) was treated with PMePh$_2$ (142 μL, 0.76 mmol) and stirred for 24 h. The solvent was evaporated from the golden-brown (toluene, benzene) or emerald-green (MeCN) solution and then the residue was treated with dry hexane (10 mL). Cooling to −4 °C produced a light-brown product, which was filtered, washed with hexane (1 mL) and ice-cold methanol (1 mL), and dried in vacuo. The yield was 174 mg (51%). Analytically pure compound may be obtained by recrystallization from dry benzene/hexane.

Preparation of solvent complexes:

[Tp^{iPr}MoOCl(NCMe)]: A sample of [Tp^{iPr}MoO$_2$Cl] (220 mg, 0.44 mmol) was dissolved in dry MeCN (15 mL) and treated with an excess of P(O*i*Pr)$_3$ (162 μL, 0.66 mmol) under argon. The stirred solution became green over 20 min. After 12 h of stirring, the solvent was evaporated and the residue was treated with hexane and cooled to −4 °C. The green crystals were filtered, washed with hexane, and dried in vacuo. The yield was 165 mg (72%).

[Tp^{iPr}MoO(SR)(NCMe)] (R = *n*Bu, *s*Bu): These compounds were synthesized by slight modification of Method A above for [Tp^{iPr}MoO(SR)(OPEt$_3$)]. Thus, the light-blue solid precipitated in the first treatment with hexane (10 mL) was immediately filtered, washed with hexane (2× 2 mL), and dried in vacuo. The yields were 50–60%.

[Tp^{iPr}MoO(S*n*Bu)(DMF)]: A solution of [Tp^{iPr}MoO$_2$(S*n*Bu)] (218 mg, 0.39 mmol) in dry DMF (20 mL) was treated with PEt$_3$ (80 μL, 0.54 mmol) and stirred for 1–2 h. The solution was then evaporated to dryness and the residue was treated with dry hexane. A light-green/blue solid precipitated immediately and was filtered, washed with cold hexane (5 mL), and dried in vacuo. The yield was 120 g (43%).

[Tp^{iPr}MoO(OAr)(NCMe)]: These complexes were formed in situ when a sample of [Tp^{iPr}MoO(OAr)(OPR$_3$)] was dissolved in dry MeCN and stirred for 1 h under anaerobic conditions. NMR spectra were recorded on samples prepared in [D$_3$]MeCN.

X-ray crystallography: Green crystals of **6** and **7** were grown by slow diffusion of hexane into a benzene solution of the compound at 4 °C. Golden crystals of **9** and **12**·0.5 C$_6$H$_6$·0.5 C$_6$H$_{14}$ were grown by the same method. Crystallographic data for all complexes are collected in Table 4 and selected metrical parameters are listed in Table 2. Unit cell parameters were obtained by a least-squares procedures from the angular settings of 25 reflections. Crystallographic data were collected on an Enraf Nonius CAD4f diffractometer by employing the ω:2θ scan method. Reflections were measured over the range $4° \le 2\theta \le 50°$ at 293(2) K by using MoKα radiation with a wavelength of 0.71069 Å. The structures were solved by direct methods and refined by using full-matrix least-squares methods on F^2 (SHELXL-97).[55] The *sec*-butyl and *n*-butyl moieties of structures **6** and **7**, respectively, were disordered. Carbon atoms of these groups were located in difference maps and, where possible, refined with partial occupancies. For the structure of **12**, the Mo–Cl and Mo–O1 bond lengths were marginally outside their expected ranges.[37] This was ascribed to a degree of disorder between the chloro and oxo ligands. However, a disordered model did not improve statistical measures of accuracy and thus was not adopted. Hydrogen atoms were included in idealized positions with the exception of the disordered *sec*-butyl group of **6** and atoms C8, C9, and C10 of the disordered *n*-butyl moiety of **7**. The atomic scattering factors used were those incorporated in the SHELXL-97 program.[55] The molecular diagrams in Figures 1–4 were generated by using the program ORTEP-3.[56]

Table 4. Crystallographic data.

Compound	**6**	**7**	**9**	**12**[a]
formula	$C_{33}H_{56}BMoN_6O_3P$	$C_{28}H_{52}BMoN_6O_2PS$	$C_{37}H_{46}BMoN_6O_3P$	$C_{42}H_{53}BClMoN_6O_2P$
formula mass	722.6	674.5	760.52	847.07
crystal system	monoclinic	monoclinic	monoclinic	triclinic
space group	$P2_1/c$	$P2_1/n$	$P2_1/n$	$P\bar{1}$
a [Å]	12.320(4)	10.4345(7)	11.7697(13)	11.122(3)
b [Å]	16.919(4)	18.7269(15)	17.707(2)	11.297(6)
c [Å]	18.854(3)	18.457(2)	18.065(4)	19.830(7)
α [°]	90	90	90	97.97(3)
β [°]	103.926(16)	103.080(7)	90.463(13)	99.74(3)
γ [°]	90	90	90	112.09(15)
V [Å^3]	3814.5(16)	3513.0(5)	3764.7(10)	2218.9(15)
Z	4	4	4	2
ρ_{calcd} [g cm^{-3}]	1.258	1.275	1.342	1.266
R	0.036	0.027	0.056	0.078
R_w	0.091	0.058	0.1318	0.1291

[a] Data for the 0.5 C$_6$H$_6$·0.5 C$_6$H$_{14}$ mixed solvate.

CCDC-257484 (**6**), CCDC-257485 (**7**), CCDC-257486 (**9**), and CCDC-257487 (solvate of **12**) contain the supplementary crystallographic data for this paper. These data can be obtained free of charge from The Cambridge Crystallographic Data Centre via www.ccdc.cam.ac.uk/data_request/cif.

Theoretical calculations: All the computations were carried out by using the Gaussian 98W or 03W[57] and HyperChem 6.03[58] software packages. For the electronic structure calculations, the starting geometries were ob-

tained from the X-ray crystal structures and used without any truncation. Becke's three-parameter hybrid exchange functional[59] and the Lee–Yang–Parr nonlocal correlation functional (B3LYP)[60] were used with the DZVP basis set on molybdenum[61] and the 6-311G(d)[62] basis sets for all other atoms. The percentage of atomic orbital contributions to their respective molecular orbitals was calculated by using the VMOdes program.[63] The results of the molecular orbital calculations are included in the Supporting Information (Tables S1–S5).

The rotational energy barriers of all complexes were calculated, starting from the X-ray crystal structures, as the energy difference between the most stable conformer and all other conformers obtained under changes in the O=Mo-O-P torsion ($\approx\pm40°$) or Mo-O-P ($\approx\pm20°$) angles with 5° increments. To reduce the steric interactions between alkyl or phenyl groups of the coordinated PR_3 ligand and isopropyl groups of pyrazole rings, these atom positions were optimized by molecular mechanics with the MM+ force field, implemented in the HyperChem package.[58] After completion of the molecular mechanics calculations, all single-point calculations were performed by using the semiempirical PM3(tm) method[64] incorporated into the HyperChem package.[58]

Acknowledgements

We thank Dr. D. Nielsen and Mr. C. Gourlay for experimental assistance and Prof. Seth Brown for helpful discussions. We gratefully acknowledge the financial support of the Australian Research Council, the University of Melbourne, the donors of the Petroleum Research Fund administered by the American Chemical Society, and the National Institutes of Health (P.B.).

[1] a) R. Hille, *Chem. Rev.* **1996**, *96*, 2757–2816; b) R. S. Pilato, E. I. Stiefel in *Bioinorganic Catalysis*, 2nd ed. (Eds.: J. Reedijk, E. Bouwman), Marcel Dekker, New York, **1999**, pp. 81–152; c) *Molybdenum and Tungsten: Their Roles in Biological Processes* (Eds.: A. Sigel, H. Sigel), "Metal Ions in Biological Systems" Series, no. 39, Marcel Dekker, New York, **2002**; d) J. M. Tunney, J. McMaster, C. D. Garner in *Comprehensive Coordination Chemistry II, Vol. 8* (Eds.: J. A. McCleverty, T. J. Meyer), Elsevier Pergamon, Amsterdam, **2004**, Chapter 8.18, pp. 459–477.

[2] a) E. I. Stiefel, *Prog. Inorg. Chem.* **1977**, *22*, 1–223; b) E. I. Stiefel in *Comprehensive Coordination Chemistry* (Eds.: G. Wilkinson, R. D. Gillard, J. A. McCleverty), Pergamon, Oxford, **1987**, Chapter 36.5, pp. 1375–1420; c) C. D. Garner, J. M. Charnock in *Comprehensive Coordination Chemistry* (Eds.: G. Wilkinson, R. D. Gillard, J. A. McCleverty), Pergamon, Oxford, **1987**, Chapter 36.4, pp. 1329–1374.

[3] C. G. Young in *Comprehensive Coordination Chemistry II*, *Vol. 4* (Eds.: J. A. McCleverty, T. J. Meyer), Elsevier Pergamon, Amsterdam, **2004**, Chapter 4.7, pp. 415–527.

[4] C. G. Young in *Biomimetic Oxidations Catalyzed by Transition Metal Complexes* (Ed.: B. Meunier), Imperial College Press, London, **2000**, p. 415–459.

[5] J. McMaster, J. M. Tunney, C. D. Garner, *Prog. Inorg. Chem.* **2004**, *52*, 539–583.

[6] J. H. Enemark, J. J. A. Cooney, J.-J. Wang, R. H. Holm, *Chem. Rev.* **2004**, *104*, 1175–1200.

[7] a) C. Kisker, H. Schindelin, A. Pacheco, W. A. Wehbi, R. M. Garrett, K. V. Rajagopolan, J. H. Enemark, D. C. Rees, *Cell* **1997**, *91*, 973–976; b) M. Czjzek, J.-P. Dos Santos, J. Pommier, G. Giordano, V. Méjean, R. Haser, *J. Mol. Biol.* **1998**, *284*, 435–447; c) A. S. McAlpine, A. G. McEwan, S. Bailey, *J. Mol. Biol.* **1998**, *275*, 613–623; d) H.-K. Li, C. Temple, K. V. Rajagopalan, H. Schindelin, *J. Am. Chem. Soc.* **2001**, *123*, 7673–7680, and references therein; e) P. J. Ellis, T. Conrads, R. Hille, R. P. Kuhn, *Structure* **2001**, *9*, 125–132; f) P. Basu, J. F. Stolz, M. T. Smith, *Curr. Sci.* **2003**, *72*, 1412–1418 (M).

[8] a) S. D. Garton, C. A. Temple, I. K. Dhawan, M. J. Barber, K. V. Rajagopalan, M. K. Johnson, *J. Biol. Chem.* **2000**, *275*, 6798–6805; b) A. V. Astashkin, M. L. Mader, A. Pacheco, J. H. Enemark, A. M. Raitsimring, *J. Am. Chem. Soc.* **2000**, *122*, 5294–5302, and references therein.

[9] M. S. Brody, R. Hille, *Biochemistry* **1999**, *38*, 6668–6677.

[10] B. E. Schultz, R. Hille, R. H. Holm, *J. Am. Chem. Soc.* **1995**, *117*, 827–828.

[11] A. Thapper, R. J. Deeth, E. Nordlander, *Inorg. Chem.* **2002**, *41*, 6695–6702.

[12] P. D. Smith, A. J. Millar, C. G. Young, A. Ghosh, P. Basu, *J. Am. Chem. Soc.* **2000**, *122*, 9298–9299.

[13] V. N. Nemykin, J. Laskin, P. Basu, *J. Am. Chem. Soc.* **2004**, *126*, 8604–8605.

[14] V. N. Nemykin, P. Basu, *Dalton Trans.* **2004**, 1928–1933.

[15] a) S. A. Roberts, C. G. Young, W. E. Cleland, Jr., R. B. Ortega, J. H. Enemark, *Inorg. Chem.* **1988**, *27*, 3044–3051; b) L. J. Laughlin, C. G. Young, *Inorg. Chem.* **1996**, *35*, 1050–1058.

[16] Z. Xiao, M. A. Bruck, J. H. Enemark, C. G. Young, A. G. Wedd, *Inorg. Chem.* **1996**, *35*, 7508–7515.

[17] a) M. A. Pietsch, M. Couty, M. B. Hall, *J. Phys. Chem.* **1995**, *99*, 16315–16319; b) M. A. Pietsch, M. B. Hall, *Inorg. Chem.* **1996**, *35*, 1273–1278.

[18] a) A. K. Rappé, W. A. Goddard, III, *J. Am. Chem. Soc.* **1982**, *104*, 448–456; b) A. K. Rappé, W. A. Goddard, III, *J. Am. Chem. Soc.* **1982**, *104*, 3287–3294.

[19] B. W. Kail, L. M. Perez, S. D. Zaric, A. J. Millar, C. G. Young, M. B. Hall, P. Basu, unpublished results.

[20] A. J. Millar, C. J. Doonan, L. J. Laughlin, E. R. T. Tiekink, C. G. Young, *Inorg. Chim. Acta* **2002**, *337*, 393–406.

[21] C. J. Doonan, PhD thesis, University of Melbourne (Parkville), **2004**.

[22] L. R. H. Hill, PhD thesis, University of Melbourne (Parkville), **2004**.

[23] P. D. Smith, D. A. Slizys, G. N. George, C. G. Young, *J. Am. Chem. Soc.* **2000**, *122*, 2946–2947.

[24] C.-S. J. Chang, J. H. Enemark, *Inorg. Chem.* **1991**, *30*, 683–688.

[25] S. B. Seymore, S. N. Brown, *Inorg. Chem.* **2000**, *39*, 325–332.

[26] M. W. G. de Bolster in *Topics in Phosphorus Chemistry*, *Vol. 11* (Eds.: M. Grayson, E. J. Griffith), Wiley-Interscience, New York, **1983**, pp. 69–296.

[27] T. S. Lobana in *The Chemistry of Organophosphorus Compounds*, *Vol. II* (Ed.: F. R. Hatley), Wiley-Interscience, Chichester, **1992**, Chapter 8.

[28] F. N. Hooge, P. J. Christen, *Recl. Trav. Chim. Pays-Bas* **1958**, *77*, 911–922.

[29] P. L. Goggin in *Comprehensive Coordination Chemistry*, *Vol. 2* (Eds.: G. Wilkinson, J. A. Gillard, J. A. McCleverty), Pergamon, Oxford, **1987**, pp. 487–503.

[30] K. Nakamoto, *Infrared and Raman Spectra of Inorganic and Coordination Compounds*, Wiley-Interscience, New York, **1986**.

[31] F. A. Cotton, R. D. Barnes, E. Bannister, *J. Chem. Soc.* **1960**, 2199–2203.

[32] G. Davidson in *The Chemistry of Organophosphorus Compounds*, *Vol. II* (Ed.: F. R. Hatley), Wiley-Interscience, Chichester, **1992**, Chapter 5.

[33] A. D. Westland, F. Haque, J.-M. Bouchard, *Inorg. Chem.* **1980**, *19*, 2255–2259.

[34] G. Aksnes, L. J. Brüdvik, *Acta Chem. Scand.* **1963**, *17*, 1616–1622.

[35] T. A. Albright, W. J. Freeman, E. E. Schweizer, *J. Org. Chem.* **1975**, *40*, 3437–3441.

[36] W. A. Nugent, J. M. Mayer, *Metal–Ligand Multiple Bonds*, Wiley, New York, **1988**.

[37] A. G. Orpen, L. Brammer, F. H. Allen, O. Kennard, D. G. Watson, R. Taylor, *J. Chem. Soc. Dalton Trans.* **1989**, S1–S83.

[38] F. A. Cotton, P. A. Kibala, C. S. Miertschin, *Inorg. Chem.* **1991**, *30*, 548–553.

[39] M. G. Crisp, L. M. Rendina, E. R. T. Tiekink, *Z. Kristallogr.* **2001**, *216*, 243–244.

[40] N. N. Greenwood, A. Earnshaw, *Chemistry of the Elements*, Pergamon, Oxford, **1984**.

[41] D. M. Baird, P. E. Fanwick, T. Barwick, *Inorg. Chem.* **1985**, *24*, 3753–3758.
[42] G. Philipp, S. Wocadlo, W. Massa, K. Dehnicke, D. Fenske, C. Maichle-Mössmer, E. Niquet, J. Strähle, *Z. Naturforsch. B* **1995**, *50*, 1–10.
[43] F. A. Cotton, M. Kohli, R. L. Luck, J. V. Silverton, *Inorg. Chem.* **1993**, *32*, 1868–1870.
[44] C. P. Brock, W. B. Schweizer, J. D. Dunitz, *J. Am. Chem. Soc.* **1985**, *107*, 6964–6970.
[45] K. Peariso, R. L. McNaughton, M. L. Kirk, *J. Am. Chem. Soc.* **2002**, *124*, 9006–9007.
[46] J. I. Detrich, R. Konecny, W. M. Vetter, D. Doren, A. L. Rheingold, K. H. Theopold, *J. Am. Chem. Soc.* **1996**, *118*, 1703–1712.
[47] T. B. Gunnoe, S. H. Meiere, M. Sabat, W. D. Harman, *Inorg. Chem.* **2000**, *39*, 6127–6130.
[48] P. Haake, R. D. Cook, G. H. Hurst, *J. Am. Chem. Soc.* **1967**, *89*, 2650–2654.
[49] V. V. Yakshkin, N. M. Meshcheryakov, M. E. Ignatov, B. I. Laskorin, V. G. Yagodin, E. G. Ilin, *Zh. Obshch. Khim.* **1985**, *55*, 1266.
[50] C. A. Tolman, *Chem. Rev.* **1977**, *77*, 313–348.
[51] T. E. Miller, D. M. P. Mingos, *Transition Met. Chem.* **1995**, *20*, 533–539.
[52] J. F. Stolz, P. Basu, *ChemBioChem* **2002**, *3*, 198–206, and references therein.
[53] *Handbook of ^{31}P Nuclear Magnetic Resonance Data*, (Ed.: J. C. Tebby), CRC Press, Boca Raton, FL, **1991**.
[54] J. C. Bryan, R. E. Stenkamp, T. H. Tulip, J. M. Mayer, *Inorg. Chem.* **1987**, *26*, 2283–2288.
[55] SHELXL-97 Program for Crystal Structure Refinement, G. M. Sheldrick, University of Göttingen, Germany, **1997**.
[56] L. J. Farrugia, *J. Appl. Crystallogr.* **1997**, *30*, 565.
[57] Gaussian 98W and Gaussian 03W, M. J. Frisch, G. W. Trucks, H. B. Schlegel, P. M. W. Gill, B. G. Johnson, M. A. Robb, J. R. Cheeseman, T. A. Keith, G. A. Petersson, J. A. Montgomery, K. Raghavachari, M. A. Al-Laham, V. G. Zakrzewski, J. V. Ortiz, J. B. Foresman, J. Cioslowski, B. B. Stefanov, A. Nanayakkara, M. Challacombe, C. Y. Peng, P. Y. Ayala, W. Chen, M. W. Wong, J. L. Andres, E. S. Replogle, R. Gomperts, R. L. Martin, D. J. Fox, J. S. Binkley, D. J. Defrees, J. Baker, J. P. Stewart, M. Head-Gordon, C. Gonzalez, J. A. Pople, Gaussian, Inc., Pittsburgh, PA, **1998**.
[58] HyperChem 6.03, HyperCube, Inc., Gainesville, FL, **2001**.
[59] A. D. Becke, *J. Chem. Phys.* **1993**, *98*, 5648–5652.
[60] C. Lee, W. Yang, R. G. Parr, *Phys. Rev. B* **1988**, *37*, 785–789.
[61] Basis sets were obtained from the Extensible Computational Chemistry Environment Basis Set Database, as developed and distributed by the Molecular Science Computing Facility, Environmental and Molecular Sciences Laboratory, which is part of the Pacific Northwest Laboratory, P. O. Box 999, Richland, WA 99352, USA, and is funded by the US Department of Energy. The Pacific Northwest Laboratory is a multiprogram laboratory operated by Battelle Memorial Institute for the US Department of Energy under contract DE-AC06–76RLO 1830. Contact David Feller or Karen Schuchardt for further information.
[62] A. D. McLean, G. S. Chandler, *J. Chem. Phys.* **1980**, *72*, 5639–5648.
[63] VMOdes: Virtual Molecular Orbital Description Program for Gaussian, GAMESS, and HyperChem, Version B6.2, V. N. Nemykin, P. Basu.
[64] J. I. P. Stewart, *J. Comput. Aided Mol. Des.* **1990**, *4*, 1–45.

Received: October 30, 2004
Published online: March 22, 2005

